Bioresource Technology 146 (2013) 704–712

Contents lists available at ScienceDirect

Bioresource Technology

journal homepage: www.elsevier.com/locate/biortech

Modeling and investigation of the channeling phenomenon in downdraft stratified gasifers

Giulio Allesina, Simone Pedrazzi *, Paolo Tartarini

Bio-Energy Efficiency Laboratory, University of Modena and Reggio Emilia, Department of Engineering 'Enzo Ferrari', Via Vignolese 905, 41125 Modena, Italy

HIGHLIGHTS

- This work is aimed at modeling the channeling phenomenon on a downdraft gasifier.
- These phenomena have been modeled and compared to experimental data.
- Results confirmed the capability of this approach to model the channeling phenomenon.
- The channeling phenomenon depends on the loading method of the gasifier.

ARTICLE INFO

Article history:
Received 13 June 2013
Received in revised form 25 July 2013
Accepted 27 July 2013
Available online 2 August 2013

Keywords:
Gasification
Channeling
Stratified reactor
Syngas
Tar

ABSTRACT

Downdraft stratified gasifiers seem to be the reactors which are most influenced by loading conditions. Moreover, the larger the reactor is, the higher the possibility to stumble across a channeling phenomenon. This high sensitivity is due to the limited thickness and superficial placement of the flaming pyrolysis layer coupled with the necessity to keep all the zones parallel for a correct running of this kind of gasifier. This study was aimed at modeling and investigating the channeling phenomenon generated by loading condition variations on a 250-kW$_e$ nominal power gasification power plant. The experimental campaign showed great variations in most of the plant outputs. These phenomena were modeled on two modified mathematical models obtained from literature. The results of the models confirmed the capability of this approach to predict the channeling phenomena and its dependency on the loading method.

© 2013 Elsevier Ltd. All rights reserved.

1. Introduction

Despite the several advantages that characterize the fluidized bed gasifiers (Knoef, 2005), fixed bed gasifiers are maintaining a high interest in the biomass market due to their simplicity, especially when operated with air as a gasification agent (Knoef, 2012; Higman and van der Burgt, 2008). However, fixed bed gasifiers are affected by various problems, such as channeling and fuel bridging.

In the bibliography, channeling can be found related to different parameters, such as the residence time (Yamazaki et al., 2005), superficial velocity (Tarhan, 2003) or devolatilization (Simone et al., 2013). In this study channeling was established working on the loading frequency of the reactor. It was proved that continuous loading of a gasifier reactor avoids strong fluctuations in the gasification performance (Reed and Das, 1988). These fluctuations are common in batch-working gasifiers due to the continuous changing of the reaction conditions (Beedie et al., 1996). Unfortunately, continuous feeding does not guarantee the complete absence of these oscillations: in concrete terms, most of the applications approximate the continuous feeding through a series of small batch loads. Every small load causes a pressure or temperature drop in the reactor, changing its internal conditions, furthermore they can force the air to pass through a few paths, causing channeling.

Gasifier design influences its sensitivity to operating conditions (Mechanical Wood Products Branch, 1986; Basu, 2010); the more distant the combustion zone is from the loading area, the less heavily the combustion reactions are influenced by the loading operations. Stratified downdraft gasifiers are characterized by the proximity of the flaming pyrolysis zone to the top surface; moreover, the drier the biomass is entering the reactor, the thinner the drying zone becomes (Reed and Das, 1988). This presumes a higher sensitivity of stratified downdraft gasifiers performance to the variations of loading operations, if compared with other typologies.

This study was aimed at modeling a 800 kW$_{th}$ stratified reactor under two different loading conditions, one of which was

---

* Corresponding author. Tel.: +39 059 205 6229; fax +39 059 205 6126.
E-mail address: simone.pedrazzi@unimore.it (S. Pedrazzi).
URL: http://www.beelab.unimore.it (S. Pedrazzi).

0960-8524/$ - see front matter © 2013 Elsevier Ltd. All rights reserved.
http://dx.doi.org/10.1016/j.biortech.2013.07.132

characterized by strong non-homogeneity of the reaction conditions inside the gasifier (due to the channeling effect). The system analyzed here consisted of a reactor able to produce up to 250 kW$_{el}$, sending the filtered syngas to two IVECO Cursor IC engines.

During the experimental campaign, the plant was run for five days, forcing the auger to load the reactor for 15 s every time the laser-meter, used for bed height control, gave the low-reactor signal. After three days of rest, the test was repeated reducing the charging time to 4 s. The system was set up fixing the power output to 160 kW$_{el}$ in order to slow down the loading operations from the nominal power conditions. Running the plant at partial power output allowed precise monitoring of the following parameters: biomass consumption, tar, water and charcoal production, superficial and inner temperatures, impeller spinning velocities and engine power output. Furthermore, the higher heating values of tar and charcoal were evaluated by experimental analysis for both operating conditions.

Results showed that the loading frequency was strongly correlated with the channeling, the explanation of the phenomenon is reported in Section 2.

2. Methods

A sketch of the analyzed power plant is reported in Fig. 1. It consists of a gasifier reactor fed with poplar woodchips; two diesel engines each set with power output to 80 kW$_e$; a cylindrical dryer, which dried the biomass using the exhaust and the cooling air of the engines. Before reaching the engines, the syngas was cleaned passing through a cyclone, a water scrubber and a battery of 24 electrostatic filters. The engines needed 5% of diesel oil to assure the ignition of the whole fuel mixture; this fuel fraction could be switched from diesel to vegetable oil after a start-up period. The reactor is shown in Fig. 2. It had a diameter of 0.92 m and it was 0.8 m high. In this kind of reactor, a coexistence of different reaction layers takes place (Pedrazzi et al., 2012; Blasi, 2000; Blasi and Branca, 2013). A stirrer placed between the flaming pyrolysis layer and the reduction layer supports the biomass mixing and avoids the formation of a biomass pile. The observed phenomena is explained here after looking locally at the processes that occurred on the reactor surface when the fresh biomass was loaded. A large amount of biomass can choke the flaming pyrolysis preventing the correct air flux to the zone. The air entering the reactor was diverted into a few paths (channels).

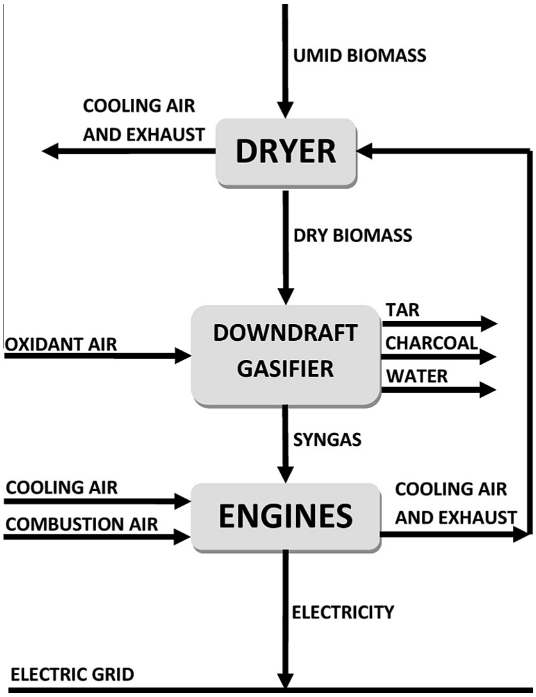

Fig. 1. Gasification system sketch.

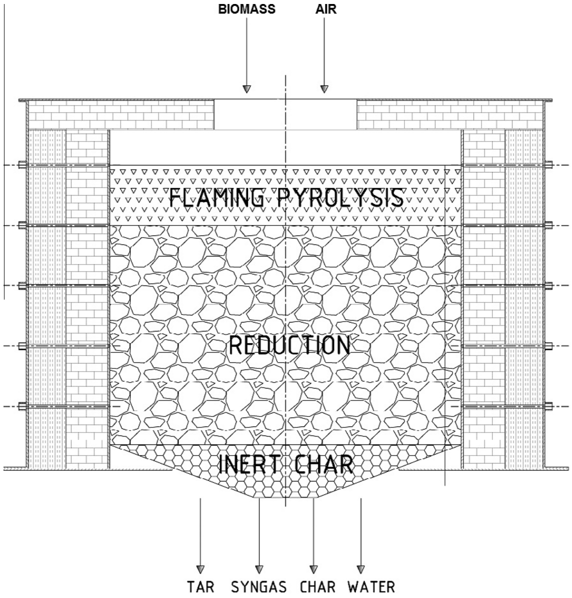

Fig. 2. Reaction design.

The previous phenomenon, well known as channeling, was reported in literature (Yamazaki et al., 2005; Tarhan, 2003; Simone et al., 2013; Dasappa et al., 2011) and it was implemented in a model specifically set up for hypothesizing the gasifier composed of two zones with different reaction conditions. The experimental data about water, tars and charcoal were compared with the model outputs in order to find out the reaction conditions of the two zones. Possible solutions capable of reducing the tar production through working on loading frequency are suggested here.

2.1. Experimental campaign

The experimental campaign discussed here is based on the experience acquired during a preliminary experimental investigation (Allesina et al., 2011) where the whole gasifier-filters-engines system was outlined an it was found to be characterized by a high inertia. The gasifier took hours to heat up properly and the filtering system discharged tars produced a long time before. For this reason the experimental campaign was designed, dividing measurements into two different categories: those obtained from the steady state plant (i.e. biomass consumption, syngas flow, temperatures, impeller spinning velocities, power output) and those obtained from the whole experimental campaign (i.e. water, char and tar production). The campaign lasted five days for every loading condition. Every day, 4 h after the plant start-up, the steady state measurements were taken.

2.2. Measurements

The gas flow rate was measured by a Pitot-tube flowmeter inserted into the pipe connecting the filtering system to the engines. The measuring point was placed about 30 diameters of rectilinear pipe away from the closest curve. In this way the average velocity in the pipe ensured a fully developed turbulent flow of syngas; this guaranteed good reliability of the measurements.

For a precise measurement of the biomass consumption, the tests were started after 4 h from plant start-up, while the plant was fed from the dryer. During the tests, the dryer was stopped and the reactor was fed with a known quantity of biomass previously dried and weighed. The average mass of poplar wood chips used for every steady-state test was about 420 kg. In order to maintain the moisture level under control, three samples of biomass were tested for every plant run using a PCE – MB 200 moisture meter. All the tested biomasses had a moisture content of under 10%. The water produced in the gasification process was collected from the water scrubber settling tank, and then it was discharged to a 1 m^3 storage tank; after every test the water level was measured and the storage tank was weighed. The top readings from the reactor temperatures were obtained with three N type 6 mm thick thermocouples. The thermocouples were placed at 10, 20 and 30 cm from the top reaction surface, the thermocouple tips were placed about 3 cm inside the reactor. The top surface temperature in the reactor was monitored continuously with a dual laser IR thermometer. Tar and char productions were collected at different points of the filtering system. The charcoal was discharged from the bottom of the reactor and the cyclone, while the tars were collected from the electrostatic filters or separated by floating or sinking in the water scrubber settling tank. These processes of separation and collection avoided an instantaneous monitoring of waste production. For this reason, the acquired data refers to five days of experimental campaign. The instantaneous power output as well as the impeller spinning velocities were obtained from the plant management software.

2.3. Ashes analysis

The biomass used in this study consisted of poplar wood chips. The main properties of the biomass are reported in Table 1. During the maintenance operation that followed the last test, some slugged ashes were found in the reactor. For this reason a sample of biomass was heat-treated in a kiln for 3 h at 550 °C in order to reduce it to ashes. Then a parallelepiped of pressed ashes was tested in an optical vertical dilatometer. The dilatometer was heated up to 500 °C and then the ashes sample was added (flash test mode as suggested by Paganelli and Sighinolfi, 2009). The temperature in the instrument rose to 850 °C at a rate of 80 °C/min and then the heaters were turned off, letting the sample cool down. Fig. 5 reports three different trends: the temperature of the sample from the moment it was inserted in the heated part of the instrument, the sintering percentage that was evaluated measuring the height variations of the sample, and the area variation that measures the crossing area of the sample. The most important trend is that of the sintering percentile. A reduction under the 95% range is symptomatic of ashes sinterization and therefore slagging is imminent. The test outlined a temperature of 750 °C, that was lower than the temperatures recorded during the tests. The presence of slags was then considered as additional proof that the reactor working on 15-s loading was characterized by the channeling phenomenon. In the channels, where the equivalence ratio is high, the temperature rose and the slags were created even if the thermocouples were recording lower temperatures in other parts of the reactor.

Table 1
Biomass proprieties.

Proximate analysis (%wt)			
Volatile matter	Fixed carbon		Ash content
79.1	18.15		2.75
Ultimate analysis (%wt)			
C	*H*		*O*
47.7	6.07		rest
Physical and chemical proprieties			
Chip equivalent diameter	d_p	0.0156	*m*
Biomass density	F_d	0.4	kg/m^3
Biomass void fraction	F_v	0.63	-
Biomass moisture	F_m	0.03	-
Dry Biomass higher heating value	$HHV_{bio,dry}$	15.67	MJ/kg

2.4. Mathematical modeling

The mathematical model was adapted from two different literature models with appropriate modifications and improvements. The first model was developed by Reed and Levie (1984); it predicts the flaming pyrolysis zone length l_p (m) and the char reduction zone length l_c (m) starting from biomass properties and gasifier dimensions with the following equations:

$$l_p = V_f t_p \tag{1}$$

$$l_c = V_f t_c \tag{2}$$

$$V_f = \frac{\dot{m}_{bio}(A_g F_d (1 - F_v))}{A_g} \tag{3}$$

where V_f is the fuel velocity (m s^{-1}), t_p is the pyrolysis time (s), t_c is the char reduction time (s), $\dot{m}_{bio}$ is the input biomass flow (kg s^{-1}), A_g is the area of the gasifier (m^2), F_d is the density of the biomass (ad) and F_v is the void fraction in the biomass (ad). The pyrolysis time t_p was obtained by the following equation (Reed and Levie, 1984):

$$t_p = \frac{F_d V (h_p + F_m h_w)}{Aq} \tag{4}$$

where V is the volume of the biomass particle (m^3), A is the surface area of the biomass particle (m^2), h_p is the heat per unit mass released by the pyrolysis process (kJ kg^{-1}) at the temperature T_s (K), h_w is the water latent heat of vaporization (kJ kg^{-1}) and q is the heat transfer rate per unit area in the pyrolysis process by radiation (kW m^{-2}). The values of h_p and h_w were tabulated by Reed and Levie (1984) starting from the data obtained by Huff (1982). The heat transfer rate q can be obtained with a weighted average calculation from the data reported by Reed and Levie (1984), where the weight of the calculation comes from the moisture of the biomass, the surface temperature and the surface area of the biomass particle. The char reduction time was calculated assuming a constant height H of the fixed bed (m) from the following equation:

$$t_c = (H - l_p)/V_f \tag{5}$$

Eqs. (1)–(5) allow a calculation of the bed and zone heights, the time of the pyrolysis process, the char reduction process assuming a constant pyrolysis surface temperature and a constant biomass consumption.

An additional approach, presented by Wang et al. (1993), was exploited to estimate the syngas composition, the air inlet flow, the syngas output flow and the charcoal and water production. This model does not consider the tar production, the temperature of the reduction zone and that the oxidant equivalence ratio are fixed. It is based on the following general reaction of gasification (Wang et al., 1993):

$$\begin{aligned} CH_\alpha O_\beta + yO_2 + zN_2 + wH_2O = {} & \phi_1 C + \phi_2 H_2 + \phi_3 CO + \phi_4 H_2O \\ & + \phi_5 CO_2 + \phi_6 CH_4 + \phi_7 N_2 \end{aligned} \tag{6}$$

where the parameters α and β can be calculated from the ultimate analysis of the biomass normalizing with the specific weight of carbon, y and z are the moles of molecular hydrogen and nitrogen for mole of biomass, these values can be calculated from the reaction balance of the biomass oxidation considering the equivalence ratio

ER defined as the ratio between the air flow and the stoichiometric air flow (Reed and Das, 1988); *w* is the number of moles of water per mole of biomass evaluated from the biomass moisture F_m, ϕ_i are the molar numbers of the products of the gasification per mole of biomass. Eq. (6) can be written in mass flow mode and it allows to calculate the syngas composition, the inlet and output flow rate assuming a constant biomass consumption. The variables ϕ_i are the unknowns of the problem. At the end of the flaming pyrolysis zone (subscript 0) these variables were calculated by solving the linear system below (Wang et al., 1993) assuming $\phi_{2,0} = 0$, $\phi_{3,0} = 0$ and $\phi_{7,0} = z$:

$$\phi_{1,0} + \phi_{5,0} + \phi_{6,0} = 1 \tag{7}$$

$$2\phi_{4,0} + 4\phi_{6,0} = \alpha + 2w \tag{8}$$

$$\phi_{4,0} + 2\phi_{5,0} = 2y + \beta + w \tag{9}$$

$$\phi_{4,0} = \lambda\phi_{5,0} + w \tag{10}$$

where $\lambda = 1$ is the ratio between water vapor and carbon dioxide formation (Wang et al., 1993). In the reduction zone the temperature decreases from 1200 K to 1000 K. Here, char is consumed gradually due to char-gas reactions and gas–gas reactions as described by the following chemical reactions (Wang et al., 1993):

1. Boudouard reaction: $C + CO_2 \rightleftarrows 2CO$
2. Water–gas reaction: $C + H_2O \rightleftarrows H_2 + CO$
3. Methanation reaction: $C + 2H_2 \rightleftarrows CH_4$
4. Steam reforming reaction: $CH_4 + H_2O \rightleftarrows CO + 3H_2$

Surface reactions 1 and 2 involve single gas molecules, while two molecules are involved in surface reactions 3 and 4. The Langmuir–Hinshelwood mechanism (Laidler, 1987) is applied to calculate the net rate for reactions 1 and 2 given by Eqs. (11) and (12), and the Langmuir–Rideal mechanism (Laidler, 1987) was adopted to calculate the net rate for reactions 3 and 4 given by Eqs. (13) and (14) as follows:

$$v_1 = -k_{a1}\frac{\phi_5 - \phi_3^2/(P_\phi K_{p1})}{\sum_{i=2}^{7}(K_i + 1/p)\phi_i}\left(\frac{\phi_{1,0}}{\phi_i}\right)^{1/3}\left(\frac{\phi_i}{\rho d_p}\right) \tag{11}$$

$$v_2 = -k_{a2}\frac{\phi_4 - \phi_2\phi_3/(P_\phi K_{p2})}{\sum_{i=2}^{7}(K_i + 1/p)\phi_i}\left(\frac{\phi_{1,0}}{\phi_i}\right)^{1/3}\left(\frac{\phi_i}{\rho d_p}\right) \tag{12}$$

$$v_3 = -k_{a3}\frac{\phi_2^2 - \phi_6 P_\phi/K_{p3}}{P_\phi K_{p1}\sum_{i=2}^{7}(K_i + 1/p)\phi_i}\left(\frac{\phi_{1,0}}{\phi_i}\right)^{1/3}\left(\frac{\phi_i}{\rho d_p}\right) \tag{13}$$

$$v_4 = -k_{a4}\frac{\phi_4\phi_6 - \phi_3\phi_2^2/(P_\phi^2 K_{p4})}{\sum_{i=2}^{7}(K_i + 1/p)\phi_i}\left(\frac{\phi_{1,0}}{\phi_i}\right)^{1/3}\left(\frac{\phi_i}{\rho d_p}\right) \tag{14}$$

$$P_\phi = \frac{1}{p}\sum_{i=2}^{7}\phi_i \tag{15}$$

where v_i is the net reaction (mol s^{-1}), k_{ai} is the apparent rate constant, K_{pi} is the equilibrium constant and K_i is the adsorption constant for the reaction i, p is the pressure in the gasifier (atm), P_ϕ is the pressure related constant obtained as described in Eq. (15), $\phi_{1,0}$ is the initial molar number of atomic carbon at the beginning of the reduction zone, ρ is the density of the atomic carbon (kg dm^{-3}), d_p is the initial equivalent diameter of the char particle (m). The equilibrium constants K_{pi} were calculated by the JANAF thermochemical tables (Sharma, 2008) and the adsorption constants K_i were taken from Everson et al. (2006) both at a fixed reduction temperature *T* (K). The apparent rate constants were calculated by the following Arrhenius equation (Dasappa et al., 2011):

$$k_{ai} = A_i \exp\left(\frac{-E_{ai}}{RT}\right) \tag{16}$$

where A_i is the pre-exponential factor (s^{-1}), E_{ai} is the activation energy (kJ mol−1) for reaction i, T is the reduction temperature and R is the universal gas constant (kJ mol−1 K−1). A_i and E_{ai} of each reaction were taken from the regression reported in Wang et al. (1993). The molar number of the products at the end of the reduction zone was obtained by integrating the following differential equations system from zero to t_c:

$$\begin{cases} \frac{d\phi_1}{dt} = v_1 + v_2 + v_3 \\ \frac{d\phi_2}{dt} = -v_2 + 2v_3 - 3v_3 \\ \frac{d\phi_3}{dt} = -2v_1 - v_2 - v_4 \\ \frac{d\phi_4}{dt} = v_2 + v_4 \\ \frac{d\phi_5}{dt} = v_1 \\ \frac{d\phi_6}{dt} = -v_3 + v_4 \end{cases} \tag{17}$$

Table 2
Model parameters.

Parameter		Value	Unit
Gasifier area	A_g	0.668	m^2
Flaming pyrolysis temperature	T_s	1173.5	K
Fixed bed height	H	0.6	m
Biomass coefficient	α	1.52	–
Biomass coefficient	β	0.67	–
Equivalence ratio	ER	0.3	–
Reduction temperature	T	1073.5	K
Pressure in the gasifier	p	1	atm
Tar higher heating value	HHV_{tar}	24.62	MJ/kg

Table 3
Comparison between the model output and the 4-s-long loading experimental data.

Variable		Model output	Experimental data	Unit
Biomass consumption	$\dot{m}_{bio}$	519	519	g/s
Syngas higher heating value	HHV_{syngas}	4.99	5.25	MJ/Nm^3
Syngas volumetric flow rate	$\dot{V}_{syngas}$	112	103	l/s
Air volumetric flow rate	$\dot{V}_{air}$	80.6	91.2	l/s
Char flow rate	$\dot{m}_{char}$	5.00	6.90	g/s
Tar + water flow rate	$\dot{m}_{tar+water}$	11.9	12.7	g/s
Cold gas efficiency	η_{gas}	66.5	66.6	%

Table 4
Comparison between the model output and the 15-s-long loading experimental data.

Parameter		Value	Unit	
Channels area	A_1	0.318	m^2	
ER of the channels area	ER_1	0.667	–	
Pyrolysis area	A_2	0.350	m^2	
ER of the pyrolysis area	ER_2	0.048	–	
Variable		Model output	Experimental data	Unit
Biomass consumption	$\dot{m}_{bio}$	531	531	g/s
Syngas higher heating value	HHV_{syngas}	4.22	3.97	MJ/Nm^3
Syngas volumetric flow rate	$\dot{V}_{syngas}$	122	103	l/s
Air volumetric rate	$\dot{V}_{air}$	87.9	91.2	l/s
Char flow rate	$\dot{m}_{char}$	6.80	7.77	g/s
Tar + water flow rate	$\dot{m}_{tar+water}$	17.3	21.8	g/s
Cold gas efficiency	η_{gas}	62.1	66.6	%

The molar flow rate of syngas, char, and water at the end of the reduction zone were evaluated using the molar mass of each product and assuming steady state conditions. Starting from the gas composition one can evaluate the syngas heating value HHV_{syngas} (MJ Nm^{-3}) thanks to Waldheim and Nilsson equation (Waldheim and Nilsson, 2001). HHV_{syngas} is used to obtain the cold gas efficiency of the reactor:

$$\eta_{gas} = \frac{\dot{V}_{syngas} HHV_{syngas}}{\dot{m}_{bio} HHV_{bio}} \tag{18}$$

where $\dot{V}_{syngas}$ is the syngas flow rate (Nm s^{-1}). Moreover the higher heating value of the biomass HHV_{bio} (MJ kg^{-1}) was calculated by Eq. (19) starting from the moisture of the biomass and the higher heating value of the dry biomass $HHV_{bio,dry}$ (MJ kg^{-1}) estimated experimentally by the Mahler bomb calorimeter (ASTM, 2007):

$$HHV_{bio} = HHV_{bio,dry}(1 - F_m) - 2.257F_m \tag{19}$$

The tar mass flow rate $\dot{m}_{tar}$ (kg s^{-1}) was evaluated using an energy balance equation:

$$\dot{m}_{tar} = \frac{\dot{V}_{syngas} HHV_{syngas} - \dot{V}_{syngas,exp} HHV_{syngas,exp}}{HHV_{tar,exp}} \tag{20}$$

where $\dot{V}_{syngas,exp}$ is the experimental volumetric flow rate, $HHV_{syngas,exp}$ is the experimental syngas higher heating value and $HHV_{tar,exp}$ is the experimental tar heating value. With this simplified approach, the tar production is evaluated looking at the differences between the quality of the modeled gas and the real gas. The basic assumption behind this method assumes that the real gasifier is not able to completely convert the biomass chemical energy into the gas chemical energy. Therefore the only loss in the conversion process is the tar production, which represents a way to discharge energy from the system.

A Matlab™software was used to implement the mathematical model discussed below. The biomass adopted in this study was wood-chip of *Popolus Alba* (Tutin and Heywo, 1976) and Table 1 collects its chemical, physical and geometrical proprieties. Table 2 shows the model input parameters, instead Tables 3 and 4 summarize the comparison between experimental data and model output. The $HHV_{bio,dry}$ and the HHV_{tar} were evaluated by a calorimetric analysis with the Mahler bomb calorimeter (ASTM, 2007).

A heuristic upgrading of the present model was employed to consider the presence of channels in the 15-s-long loading operation mode. The channels were modeled considering them as a part of the reactor with a total area A_1, while the rest of the reactor bed was assumed to have a section with total area $A_2 = A - A_1$. Biomass consumption in each sub-reactor was considered proportional to its area. Each part was simulated with different boundary conditions: ER_1, $\dot{m}_1 = \dot{m}A_1/A$ for the first part; ER_2, $\dot{m}_2 = \dot{m}A_2/A$ for the second part. A method that randomly changed the boundary conditions was applied to verify if the channeling theory could explain both the high water and tar production. Table 4 collects the

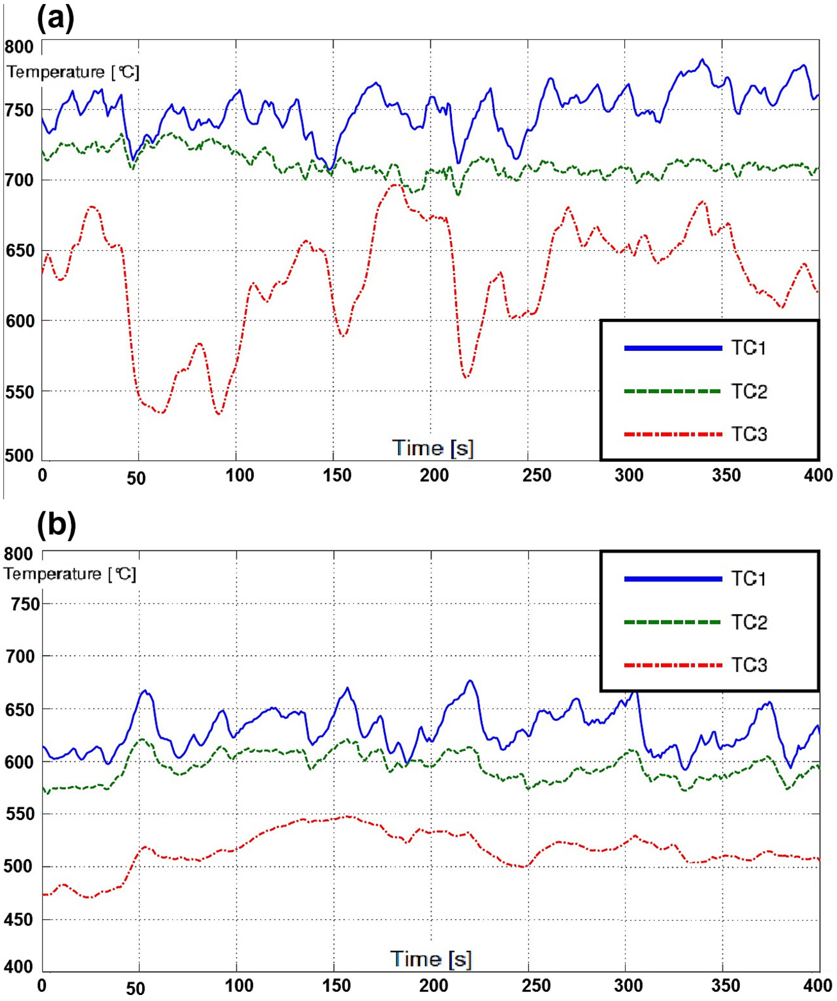

Fig. 3. Thermal stratigraphy in the 4-s-long loading test (a) and in the 15-s-long loading test (b).

boundary conditions that better fit with the experimental output. This approach went under the name of the ‘inception model’ because it simulated the presence of a gasifier within a gasifier.

3. Results and discussion

3.1. Temperature

The thermal stratigraphy of the top part of the gasifier is reported in Fig. 3. The temperatures were lower than what literature suggests in both the loading conditions. The temperature in the center of the reactor should have been higher than that which was attained by the thermocouples because the reactor diameter was big and the biomass could not properly reach the peripheral part of the gasifier. Here the biomass created a small ash annulus that protected the thermocouples from the higher temperature of the gasifier. During the plant maintenance operations, the ash layer was measured and it proved to be a maximum of 3 cm thick. The reduced thickness justifies that this phenomenon was in fact ignored in the model.

Fig. 3 shows the different temperature trends at the top of the reactor for the two loading conditions. In the 15-s-load feed (Fig. 3 (b)), the large amount of biomass for every “batch” decreased the reactor temperature due to the sensitive heat absorbed by the biomass and choked the flaming combustion reactions on the top surface of the reactor bed. The 15-s-long loading test showed lower temperatures and small fluctuations, especially for the thermocouple placed under the flaming pyrolysis zone (TC-3). In fact, the reactor was not able to recover the high temperature suggested by literature for these zones. The 4-s-long loading condition created greatly fluctuating high temperatures, even for the deeper thermocouple. These variations were related to an irregular gasification zone: the width of the peaks was about 60 s, this was the stand-by period for every 5 s run of the stirrer. In the 15-s test, the thermal substratum had a low temperature and was quite homogeneous; for this reason the stirrer did not create significant variations, but during the 4-s test (Fig. 3(a)) this substratum was characterized by higher temperatures ranging from 500 to 700 °C, which are the extremes of gasification reaction temperatures as reported by Reed and Das (1988), Higman and van der Burgt (2008) and Knoef (2005).

Such a non-homogeneous zone was greatly modified by the passage of the stirrer, thus justifying the significant variations. Fig. 4 shows two trends obtained acquiring the superficial temperature of the reacting bed with the IR thermometer. The thermometer was a dual laser infrared thermometer with focus 50:1 inches fixed on the air inlet chimney, focusing it on the top of the reacting surface.

The differences between Fig. 4(a) and (b) consist in the maximum temperature reached by the surfaces; furthermore the temperature recovery was slower in the 15 s loading. The 15 s loading showed 9 big peaks during the 1000 s of the screenshot, it resulted in a 15 s long loading every 111 s. For the 4-s test this value decreased to 77 s on average. In order to estimate the

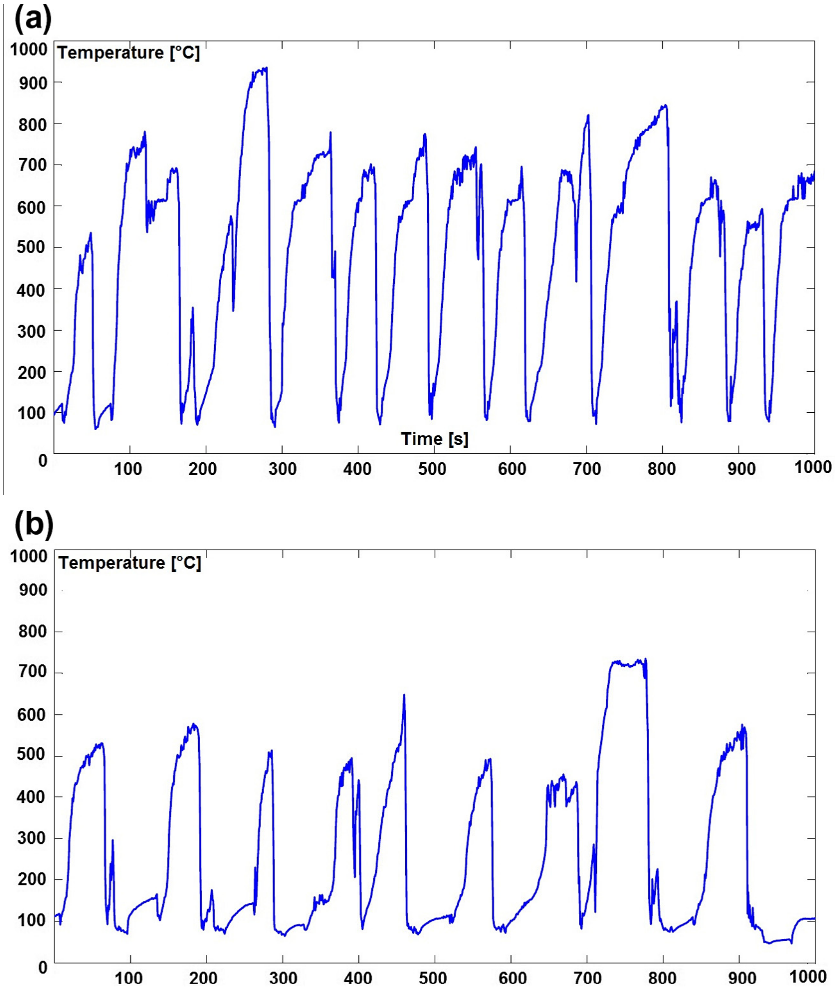

Fig. 4. Superficial temperature in the 4-s-long loading test (a) and in the 15-s-long loading test (b).

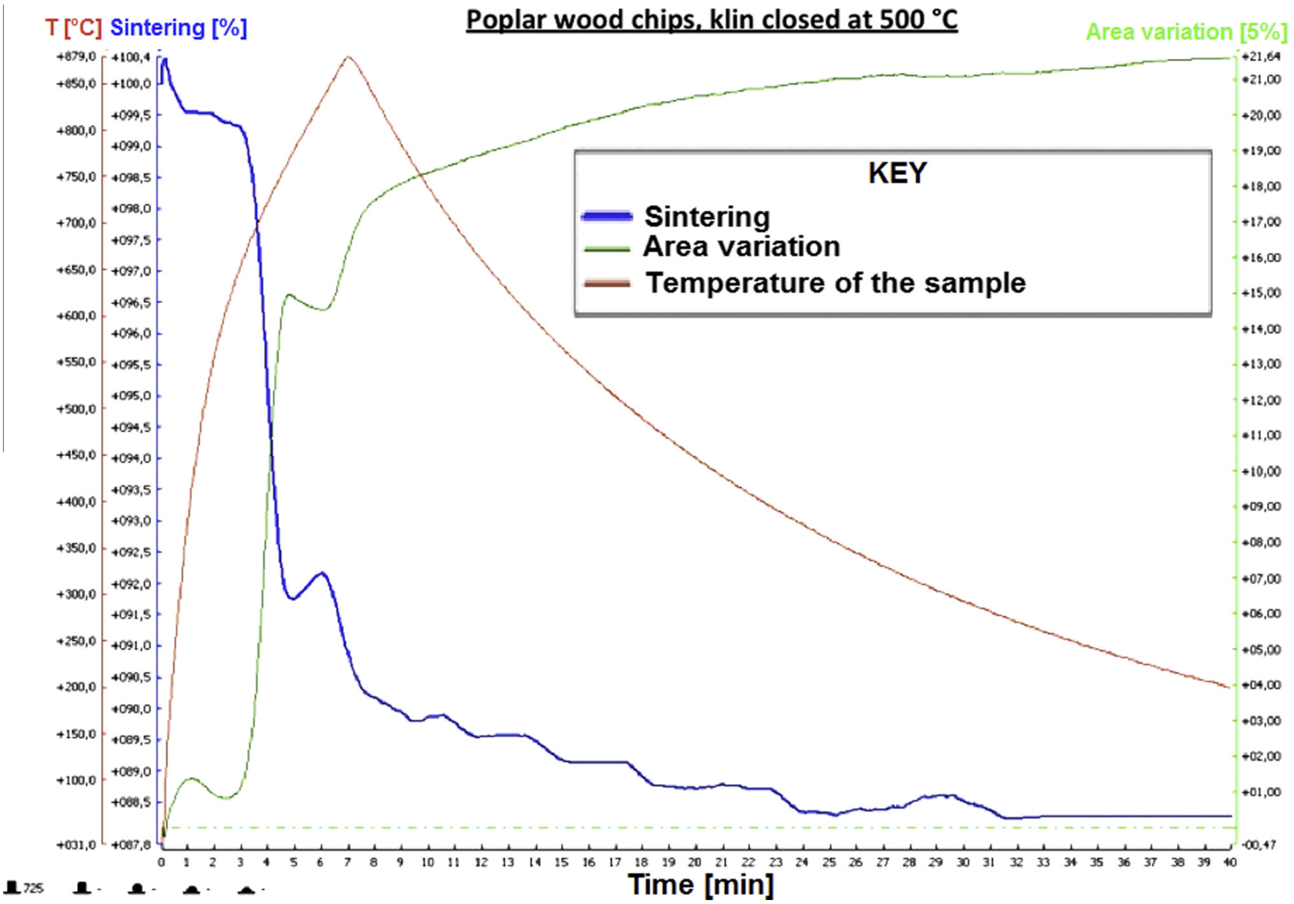

Fig. 5. Optical dilatometer ashes test.

amount of time in which the combustion reactions were locally choked due to the sudden loading, the temperature trends were divided into two zones: above and below 250 °C. This value was the average autoignition temperature for wood (Babrauskas, 2001); for this reason, during the periods with a reactor surface temperature above 250 °C, a wood parcel on the top surface could start its flaming pyrolysis if it was able to reach the right amount of oxidant. Results of this analysis are reported in Table 5. The 4-s loading condition resulted in a surface reactor temperature above the autoignition one for the 67% of the duration of the test. During the 15-s-loading campaign this value was lower (39% of the duration of the test). A lower value can be related to a higher tar production because temperatures under 250 °C, associated with the choking effect of long loading, generate a more similar reaction to the torrefaction than to that of flaming pyrolysis (Prins et al., 2006).

Table 5
Superficial temperature of the reacting bed comparison.

Variable		4 s load	15 s load	Unit
Fraction time over 250 °C	t_{hot}	67.89	38.6	%
Minimum average temperature	T_{min}	42.6	31.8	°C
Maximum average temperature	T_{max}	896	739	°C
Average temperature	T_{mean}	422	259	°C

3.2. Power output and propeller frequencies

The power plant studied here is controlled on a power output basis. Once the power output was set, the controller continuously changed the impeller frequencies, increasing or decreasing the amount of syngas drawn from the reactor and sent to the engines, in order to maintain the fixed power generation. Changing the syngas flow, constantly modified the reaction conditions. This phenomenon created oscillations in the propeller frequency and in the instantaneous power output registered from the controller data logger.

In order to quantify differences in the instability of the whole system under the two loading conditions, the instantaneous values of the impeller spinning frequencies and power output were acquired. The mean value and the standard deviation were calculated and reported in Table 6. For the 15-s loading the impellers spun faster on average. This can be related to a poorer quality of syngas because a greater amount of gas was necessary for the same power output. Moreover, the standard deviation of the spinning frequency was also higher in this case. This suggests that the great thermal and physical oscillations at the top of the reactor influenced the behavior of the propellers too. The result obtained for the power output was different and Table 6 shows a lower standard deviation of this parameter in the 15-s loading. This phenomenon can be explained looking at the temperature trends in Fig. 4: during this loading condition the temperatures rose slowly after every reactor refill. For this reason, even if the impellers were forced to greatly change their spinning velocities due to the large changes in the reacting conditions, these changes occured slowly, so the impellers could properly “follow” the changes maintaining a more constant power output.

Table 6
Propeller frequencies comparison and engines output comparison.

Variable		4 s load	15 s load	Unit
Minimum average propeller frequencies	f_{min}	21.4	21.3	Hz
Maximum average propeller frequencies	f_{max}	37.8	38.9	Hz
Average propeller frequencies	f_{mean}	29.9	30.78	Hz
Standard deviation of the propeller frequencies	$std.f_{mean}$	2.71	3.08	Hz
Minimum average electrical power	P_{min}	119.5	116.6	kW
Maximum average electrical power	P_{max}	207.7	204.6	kW
Average electrical power	P_{mean}	158.2	158.5	kW
Standard deviation of the electrical power	std, P_{mean}	4.79	4.17	kW

3.3. Model and experimental output

Tables 3 and 4 collect the main outputs for the two different loading conditions compared with the analogous simulated system. The more important data for channeling monitoring were the water production and the tar production, they can be considered in contrast with each other because a higher equivalence ratio causes low tar and high water production due to the preponderance of the combustion reactions. The opposite condition is related to a low equivalence ratio that produces oils and tars instead of water. The 15-s-loading campaign resulted in a high production of both water and tar. The scientific explanation came from the ‘inception’ model of the reactor, which simulated a reactor characterized by the coexistence of combustion paths in channels while the rest of the reactor works with a low equivalence ratio condition. Table 3 shows the effectiveness of the model adopted for the prediction of the main parameters that characterized the reactor without channeling, while Table 4 shows how the model divided the reactor in order to match the experimental data. The model suggested an almost equal division of the reactor area with completely different equivalence ratios. Under these conditions half of the gasifier acted as a pyrolysis reactor producing high amounts of tar. The rest of the gasifier was responsible for the water and ash slags production.

Despite the presence of a double bladed stirrer in the reactor, which had the purpose of increasing the fuel flow and reducing the channeling (Patil et al., 2011; Ma et al., 2012), this phenomenon still affected the gasifier. This could have been caused by a peripheral location of channels, but the low temperatures recorded through the reactor jacket suggested abandoning this hypothesis. A possible interpretation of the presence of the channeling even in a gasifier equipped with a stirrer consisted in a synergy of two factors: first of all, due to the particular air inlet design, the flaming pyrolysis zone was not flat and the stirrer could contribute to damaging the fragile equilibrium of this thermal zone. Moreover the channeling formation rate may have been faster than the capability of the stirrer to desegregate the channels. These observations outlined the importance of working on control parameters and modeling before designing structural modifications to the plant or the reactor; the results reported here show how the subdivision of the loading in small amounts drastically reduced the tar formation and the water production in the reactor.

3.4. Biomass consumption and char production

Comparing the two tables, the amount of biomass consumed per hour did not seem to be influenced by the loading conditions and it depended only on the set power output of the whole system.

The charcoal production required particular careful because it was similar under the two conditions. This is somehow an unexpected result, because a higher amount of energy was presumed to be discharged by the char in the 15-s-loading case. For this reason, the different charcoals were tested in a bomb calorimeter in order to estimate their high heating value. The charcoal produced during the 15-s loading test had a HHV of 24.87 MJ kg^{-1}, higher than the 17.89 MJ kg^{-1} obtained testing the charcoal produced during the 4-s loading test. This phenomenon was caused by the char discharging system, which worked maintaining a fixed pressure drop at the bottom of the reactor, ignoring the fact that the char had or had not finished reacting.

4. Conclusions

The experimental campaign showed a significant relationship between loading parameters and channeling phenomenon in downdraft gasifiers. Contemporaneously to these investigations, the channeling produced by loading the reactor with 15 s-long batches found a theoretical counterpart thanks to the “inception” mathematical model. This model explained the effect of large loads that choke the superficial reactions, forcing the air to run through a few paths in the reacting bed. Channels generated in such a way are characterized by a high equivalence ratio where most of the water is produced, while the rest of the reactor runs with a low equivalence ratio, producing a great amount of tar.

References

Allesina, G., Pedrazzi, S., Cattini, C., 2011. Experimental assessment and modeling of energy conversion effectiveness in a gasification power plant. Int. J. Heat Technol. 29, 151–156.

ASTM, 2007. ASTM D240-09 standard test method for heat of combustion of liquid hydrocarbon fuels by bomb calorimeter. Technical Report, ASTM International.

Babrauskas, V., 2001. Ignition of wood: a review of the state of the art. In: Interflam. Interscience Communications Ltd., London.

Basu, P., 2010. Biomass Gasification and Pyrolysis: Practical Design and Theory. Academic Press, Elsevier.

Beedie, D., Bowen, P., O’Dohery, T., Syred, N., 1996. Cyclic variations and control of a batch biomass gasifier-combustor. Combust. Sci. Technol. 1, 529–556.

Blasi, C.D., 2000. Dynamic behaviour of stratified downdraft gasifiers. Chem. Eng. Sci. 55, 2931–2944.

Blasi, C.D., Branca, C., 2013. Modeling a stratified downdraft wood gasifier with primary and secondary air entry. Fuel 104, 847–860.

Dasappa, S., Sridhar, H.V., Sridhar, G., Paul, P.J., 2011. Science and technology aspects of bio-residue gasification. Biomass Convers. Biorefin. 1, 121–131.

Everson, R.C., Neomagus, H.V.J.P., Kasaini, H., Njapha, D., 2006. Reaction kinetics of pulverized coal-chars derived from inertinite-rich coal discards: gasification with carbon dioxide and steam. Fuel 85, 1076–1082.

Higman, C., van der Burgt, M., 2008. Gasification. GPP.

Huff, E., 1982. Effect of size, shape, density, moisture and furnace wall temperature on burning time of wood pieces. In: Fundamentals of Thermo-Chemical Biomass Conversion: An International Conference, Estes Park, CO.

Knoef, H., 2005. Handbook of Biomass Gasification. BTG.

Knoef, H., 2012. Handbook of Biomass Gasification, second ed. BTG.

Laidler, K.J., 1987. Chemical Kinetics. Harper sRow Publishers, New York.

Ma, Z., Zhang, Y., Zhang, Q., Qu, Y., Zhou, J., Qin, H., 2012. Design and experimental investigation of a 190 kwe biomass fixed bed gasification and polygeneration pilot plant using a double air stage downdraft approach. Energy 46 (1), 140–147.

Mechanical Wood Products Branch, F.F.D., 1986. Woodgas as engine fuel. vol. ISBN 92-5-102436-7. F.A.O.

Paganelli, M., Sighinolfi, D., 2009. New double optic heating microscope for multi-standard analysis. CFI, Ceram. Forum Int. 86 (5), E18–E21.

Patil, K., Bhoi, P., Huhnke, R., Bellmer, D., 2011. Biomass downdraft gasifier with internal cyclonic combustion chamber: design, construction, and experimental results. Bioresour. Technol. 102, 6286–6290.

Pedrazzi, S., Allesina, G., Tartarini, P., 2012. Aige conference: a kinetic model for a stratified downdraft gasifier experimental assessment and modeling of energy conversion effectiveness in a gasification power plant. Int. J. Heat Technol. 30, 41–44.

Prins, M.J., Ptasinski, K.J., Janssen, F.J., 2006. Torrefaction of wood. Part 1: Weight loss kinetics. J. Anal. Appl. Pyrolysis 77, 28–34.

Reed, T., Levie, B., 1984. A simplified model of the stratified downdraft gasifier. International Bio-Energy Directory and Handbook, The Bio-Enegy Council, New York (Washington D.C.), pp. 379–389.

Reed, T.B., Das, A., 1988. Handbook of Biomass Downdraft Gasifier Engine Systems. The Biomass Energy Foundation Press.

Sharma, A.K., 2008. Equilibrium and kinetic modeling of char reduction reactions in a downdraft biomass gasifier: A comparison. Sol. Energy 82, 918–928.

Simone, M., Barontini, F., Nicolella, C., Tognotti, L., 2013. Assessment of syngas composition variability in a pilot-scale downdraft biomass gasifier by an extended equilibrium model. Bioresour. Technol. 140, 43–52.

Tarhan, S., 2003. Airflow channeling through fixed wheat straw bed in an updraft gasifier before the initiation of gasification. Energy Sour. 25 (12), 1183–1191.

Tutin, T., Heywo, V., 1976. Flora Europea. Cambridge University Press.

Waldheim, L., Nilsson, T., 2001. Heating value of gases from biomass gasification. Technical Report, IEA Bioenergy Agreement, Task 20 – Thermal Gasification of Biomass.

Wang, Y., Kinoshita, C., 1993. Kinetic model of biomass gasification. Sol. Energy 51, 19–25.

Yamazaki, T., Kozu, H., Yamagata, S., Murao, N., Ohta, S., Shiya, S., Ohba, T., 2005. Effect of superficial velocity on tar from downdraft gasification of biomass. Energy Fuels 19, 1186–1191.